A Study of the Coordination Geometry of the Tetrapyridine Copper(II) Complex in NaY and MCM-41 by Two-Dimensional Electron Spin Resonance HYSCORE Spectroscopy

A. Pöppl,[†] M. Gutjahr,[†] M. Hartmann,[‡] W. Böhlmann,[†] and R. Böttcher*,[†]

Fakultät für Physik und Geowissenschaften, Universität Leipzig, Linnéstrasse 5, D-04103 Leipzig, Germany, and Institut für Technische Chemie I, Universität Stuttgart, D-70550 Stuttgart, Germany

Received: May 7, 1998; In Final Form: July 21, 1998

The coordination geometry of the tetrapyridine copper(II) complex in zeolite Cu−NaY and mesoporous siliceous MCM-41 material is investigated by two-dimensional proton and deuterium hyperfine sublevel correlation (HYSCORE) spectroscopy. Different orientations of the pyridine ligands with respect to the complex plane of the tetrapyridine copper(II) complex were found in the two materials. The ligands are predominately arranged with their molecular plane perpendicular to the complex plane in zeolite Cu−NaY. Otherwise, in Cu−MCM-41 materials the ligands have a mean orientation of their molecular plane parallel to the complex plane. However, the two-dimensional hyperfine sublevel correlation spectra reveal severe distortions of the overall complex. The different coordination geometries of the tetrapyridine copper(II) complex in both materials result from the interaction of the complex with the inner surface of each molecular sieve. Consequently, much severe distortion of the complex geometry was found in the mesoporous Cu−MCM-41 material with its amorphous wall structure in comparison to crystalline Y zeolite. The incorporation of the tetrapyridine Cu(II) complex into Y zeolite also alters the electron spin density distribution within the complex. The results indicate a substantial influence of the framework of the Y zeolite on the unpaired electron of the encapsulated complex.

Introduction

A major challenge in the research on porous materials is the incorporation of organometallic compounds into molecular sieve materials to generate specific catalysts and nanostructured materials for potentially novel optical and electronic applications.[1] Various molecular sieves such as aluminosilcates, aluminophosphates, and mesoporous MCM-41 have been used as host materials.[2,3] Zeolites, AlPOs, and SAPOs possess well-defined sites for metal complexes owing to their crystalline structure.[1] However, the size of the cages and channels is limited to ranges between about 4 and 13 Å depending on the type of molecular sieve. The limited channel and cage dimensions often prevent the usage of these crystalline structures for incorporation of large complexes and catalytical applications involving large molecules. The novel mesoporous MCM-41 materials offer the potential to overcome this disadvantage. MCM-41 is composed of a hexagonal array of uniformly sized silica tubes with an internal diameter of about 30 Å.[4] An exciting property of these mesoporous materials is the possibility to control the pore size in the range between 20 and 100 Å by variation of the synthesis conditions.[4,5] However, the sites are poorly defined since the silicon dioxide in the walls surrounding the tubes has an amorphous structure.[4,6] But potential application of such host−guest systems in catalysis and material engineering requires detailed characterization of the site of the metal complexes and their overall coordination geometry, including the arrangement of the ligands. The investigation of metal complexes encapsulated in the pores of molecular sieve materials is also of fundamental interest in the study of host−guest systems.[1] For most of the interesting complexes, molecular sieves exist with pore diameters that are in the range of the complex dimensions. Therefore, the influence of spatial constraints on the complex symmetry can be examined by using molecular sieves with different pore sizes. Furthermore, the usage of molecular sieves with various silicon/aluminum ratios allows the study of the effect of the electrostatic potential at the site on the electron density distribution within the complex.

Immobilized copper(II) pyridine complexes are of particular interest because of their catalytic activity in oxidative coupling reactions[7] and their flexibility in the ligand arrangement, which allows the study of spatial constraints in a very detailed manner. It is also noteworthy that complexes with an unusual number of two,[8] three,[9,10] or five[11] coordinated pyridine molecules have been detected, depending on the relative coordination strength of the structural oxygens and the pore diameter of the host materials.

Typical analytical tools for the characterization of encapsulated metal complexes are optical spectroscopy, XPS, EXFAS, and XRD techniques,[1] which need rather high loadings. If the metal ion is paramagnetic as in the case of the Cu(II) pyridine complexes, the encapsulated species can be studied by electron spin resonance (ESR) spectroscopy. The various ESR techniques provide unique information about the coordination symmetry and ligand arrangement even for low concentrations owing to their high sensitivity and spectral resolution. For instance, the coordination symmetry of the cupric ion itself can be deduced from the Cu(II) electron Zeman interaction tensor **g** and the metal ion hyperfine (hf) interaction tensor $\mathbf{A}^{\mathbf{Cu}}$. Both quantities can be determined from a continuous wave (CW) ESR experiment.

Copper(II) pyridine complexes with different numbers of coordinated pyridine molecules have been studied in various molecular sieve materials such as NaX,[12] NaY,[13,14] ZSM-5[8,9]

[†] Universität Leipzig.
[‡] Universität Stuttgart.

S1089-5647(98)02170-1 CCC: $15.00
Published on Web 09/12/1998

zeolites, VPI-5,[15] SAPO-n,[10,15] pillared clays11 and MCM-41[16] by means of CW ESR. Among these host materials the formation of the common tetrapyridine copper(II) complex could only be detected in NaX, NaY, pillared clays, and MCM-41 on the basis of the number of resolved nitrogen super hyperfine (shf) structure lines in the ESR spectrum. However, the spectral resolution of the CW ESR spectroscopy was not sufficient in these experiments to resolve weak hf interactions between the paramagnetic ion and proton ligand nuclei, which are necessary to deduce the overall structure of the complex and its electron spin density distribution. Electron nuclear double resonance (ENDOR)[17] and electron spin echo envelope modulation (ESEEM)[18] methods offer the potential to overcome this disadvantage. Both techniques provide information about the number and arrangement of the ligands via the measurements of small hf and nuclear quadrupole (nq) interaction, which are usually hidden in the line width of the ESR powder pattern. Especially ESEEM methods has been proven to be very useful for the measurement of small hf and nq couplings in disordered systems such as microporous materials.[19] One approach is the direct analysis of the time domain ESEEM pattern usually measured by two or three pulse sequences.[20] Using a spherical averaging approximation, the number of interacting ligand nuclei and their dipolar (hf) interaction can be evaluated by a simulation of the time domain ESEEM spectra with high accuracy as shown in a variety of studies on metal oxide surfaces.[19] However, this approach does not allow a direct determination of the coordination geometry of the nuclei from ESEEM spectra, since geometrical correlations between the interacting nuclei are not included in the spherical averaging approximation used to analyze the powder spectra. Furthermore, the analysis of the ESEEM time domain signal often leads to erroneous results for Cu(II) complexes involving nitrogen-coordinated ligands. This is probably caused by a relatively large delocalization of the unpaired spin into the ligands.[21]

Two-dimensional (2D) ESEEM sequences such as the 2D four-pulse or HYSCORE (hyperfine sublevel correlation spectroscopy) experiment[22] have the potential to overcome these problems. In the HYSCORE experiment ($\pi/2-\tau-\pi/2-t_1-\pi-t_2-\pi/2-\tau-$echo), the mixing π-pulse creates correlations between nuclear coherences of two different electron spin (M_S) manifolds with the nuclear transition frequencies ω_{ij} and ω_{lm}. These correlations lead to cross-peaks (ω_{ij}, ω_{lm}), (ω_{lm}, ω_{ij}), or ($-\omega_{ij}$, ω_{lm}), ($-\omega_{lm}$, ω_{ij}) in the 2D Fourier-transformed (FT) spectra depending on the size of the hf and nq interaction with respect to the nuclear Larmor frequency. The spread of the ESEEM pattern into two dimensions improves significantly the spectral resolution of the FT ESEEM spectrum. In disordered systems, where the anisotropy of the hf and nq interaction results in a spread of the nuclear transition frequencies, the correlations between ω_{ij} and ω_{lm} lead to ridge-type cross-peaks.[23] These cross-peak ridges are well-separated in many experimental cases. In such spectra the hf and nq parameters can be determined by analysis of the position and shape of those ridges.[23−25] Therefore, the 2D techniques provide more spectral information, especially in disordered systems, than 1D experiments, where only broad featureless signals are observed in many spectra.

In this paper, we use orientation selective proton and deuterium HYSCORE spectroscopy to explore the coordination geometry of the tetrapyridine copper(II) complexes in Cu−NaY and Cu−MCM-41 materials. The experiments allow the study of the orientation of the pyridine ligands with respect to the coordinate frame of the electron Zeeman interaction tensor **g** of the cupric ion. The results are supported by simulations of the proton and deuterium HYSCORE powder spectra. A comparison of the ligand arrangement of the complex incorporated into both materials provides information about spatial constraints on the complexes in the two molecular sieve materials. In the case of the crystalline Cu−NaY zeolite, we can determine the preferential location of the tetrapyridine copper(II) complex from the determined overall complex symmetry and sterical arguments.

Orientation Selective HYSCORE Spectroscopy

The orientation selective HYSCORE spectroscopy of transition metal ion complexes with $S = {}^1/_2$, $I = {}^1/_2$ spin systems and axially symmetric **g** and proton hf interaction tensors **A** has been discussed in detail in a previous paper.[24] Nevertheless, it seems to be useful for the understanding of the presented results to summarize the main features. If we describe the dipolar hf interaction by a point dipole approximation, the nuclear transition frequencies ω_α and ω_β are given by[26]

$$\omega_{\alpha/\beta} = [(\omega_I \mp A/2)^2 + (B/2)^2]^{1/2} \quad (1)$$

with the parameters

$$A = 2\pi T_\perp[(3/g^2)(g_{||}^2 \cos\theta_g \cos\theta_I + g_\perp^2 \sin\theta_g \sin\theta_I \cos\phi_I) \times (\cos\theta_g \cos\theta_I + \sin\theta_g \sin\theta_I \cos\phi_I) - 1] + 2\pi A_{iso} \quad (2)$$

$$B^2 = B'^2 + C'^2 \quad (3)$$

$$B' = 2\pi T_\perp[(3/g^2)(g_{||}^2 \cos\theta_g \cos\theta_I + g_\perp^2 \sin\theta_g \sin\theta_I \cos\phi_I) \times (\cos\theta_g \sin\theta_I \cos\phi_I - \sin\theta_g \cos\theta_I) + (A_{iso}/T_\perp - 1)(g_\perp^2 - g_{||}^2)/g^2 \sin\theta_g \cos\theta_g] \quad (4)$$

$$C' = 2\pi T_\perp[(3/g^2)(g_{||}^2 \cos\theta_g \cos\theta_I + g_\perp^2 \sin^2\theta_g \sin\theta_I \cos\phi_I)(\sin\theta_I \sin\phi_I)] \quad (5)$$

and

$$T_\perp = g g_n \beta \beta_n / hr^3 \quad (6)$$

$$g^2 = g_{||}^2 \cos^2\theta_g + g_\perp^2 \sin^2\theta_g \quad (7)$$

Here, A_{iso} and $T_\perp$ are the isotropic and dipolar hf coupling parameters, which are related to the principal values of the hf interaction tensor **A** by $A_{zz} = A_{iso} + 2T_\perp$, and $A_{xx/yy} = A_{iso} - T_\perp$. The quantities $g_{||}$ and $g_\perp$ are the principal values of the **g** tensor, and ω_I is the Larmor frequency of the coupled nucleus. The other terms are defined as illustrated in Figure 1. The $g_{||}$ axis of the Cu(II) **g** tensor frame is directed perpendicular to the complex plane, which is defined by the Cu−N bond directions. The $g_\perp$ axes are within the complex plane. The *z* axis of the hf interaction tensor is assumed to point along a vector that joins the electron spin and the nucleus, where *r* is the distance between electron spin and the nucleus. The coordinate system is chosen such that that the *z* axis of the hf tensor lies in a plane defined by the $g_{||}$ and $g_\perp$ axis at angle θ_I to the $g_{||}$ axis. The quantity ϕ_I is the azimuthal angle about $g_{||}$ between the $g_{||} - g_\perp$ plane and the $g_{||}-\boldsymbol{B}_0$ plane. The polar angle θ_g between the $g_{||}$ axis and $\boldsymbol{B}_0$ in the $g_{||} - \boldsymbol{B}_0$ plane is controlled by selecting proper field settings for the microwave

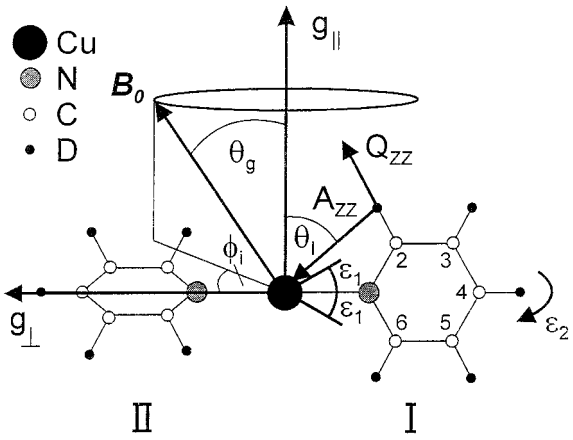

Figure 1. Schematic drawing of the tetrapyridine copper(II) complex together with a vector diagram showing the relationship between the external magnetic field $\mathbf{B}_0$, the **g** tensor frame and the *z* axis of the hf and nq interaction tensors. The $g_\perp$ and $g_{||}$ axis of the Cu(II) **g** tensor frame are perpendicular and parallel to the complex plane, respectively. Only two pyridine ligand molecules are shown for simplification. The numbers label the different positions of carbon and proton/deuterium atoms in the pyridine ligand. The angles ϵ_1 and ϵ_2 describe the two degrees of disorder in the arrangement of the pyridine ligands. ϵ_1 measures the tilt of the Cu−N bond out of the complex plane, and ϵ_2 is the rotation angle about the Cu−N bond direction.

irradiation within the anisotropic ESR powder pattern. Note that $\boldsymbol{B}_0$ may have any orientation in an annulus cut from a sphere about the $g_{||}$ axis in the orientation-selective spectrum of a powder sample. This gives rise to a spread in the nuclear transition frequencies, which in turn leads together with the correlations between ω_α and ω_β to the ridge-type shape of the cross-peaks in the HYSCORE spectrum.[23] These cross-peak ridges are directed perpendicular to the frequency diagonal axis $\omega_1 = \omega_2$ in the 2D spectrum in the case of small hf interaction, $2\pi T_\perp + \pi A_{iso} < \omega_I$. The second-order parameter B in eq 1 causes a shift $\Delta\omega^S$ of the ridges from the $\omega_1 = -\omega_2$ axis toward higher frequencies.[23,24] In the following we want to restrict ourselves to the case $A_{iso} > 0$, which is relevant for the proton nuclei in the pyridine ligand molecules of the tetrapyridine Cu(II) complex.[24] If $\theta_I > 45°$, both $T_\perp$ and A_{iso} can be estimated from a spectrum taken at the $g_\perp$ spectral position ($\theta_g = 90°$) of the ESR powder pattern. The dipolar coupling parameter $T_\perp$ is determined from the maximum vertical shift $\Delta\omega^S_{max}$ of the cross-peak ridges from the $\omega_1 = -\omega_2$ axis according to[24]

$$T_\perp = (2/3)[(8\Delta\omega^S_{max}\omega_I)/(2^{1/2}4\pi^2)]^{1/2} \quad (8)$$

Then, A_{iso} can be extracted from the inner end position of the ridges (ω^i_α, ω^i_β) and (ω^i_β, ω^i_α), which correspond to the canonical orientations $A_{xx/yy}$ of the hf tensor ($\theta_I = 90°$) using the expression

$$\omega^i_{\alpha/\beta} = \omega_I + \pi(-T_\perp + A_{iso}) \quad (9)$$

If $\theta_I < 45°$, A_{iso} can be still taken from the $g_\perp$ spectrum according to eq 9, but spectra have to be measured at other field positions $\theta_g < 90°$ to find the maximum shift $\Delta\omega^S_{max}$ of the ridges for the determination of $T_\perp$. The outer end positions of the ridges (ω^0_α,ω^0_β) and (ω^0_β,ω^0_α), which correspond to orientations $\phi_I = 0$, depend on the orientation of the *z* axis of the hf interaction tensor with respect to the **g** tensor frame. Differences of 20° between θ_g and θ_I give already significant effects on the outer end positions of the cross-peak ridges.[24] It is worth mentioning that (ω^0_α,ω^0_β) and (ω^0_β,ω^0_α) are only a measure for the canonical orientation A_{zz} when $\theta_g = \theta_I$. Then,

$$\omega^0_{\alpha/\beta} = \omega_1 + \pi(2T_\perp + A_{iso}) \quad (10)$$

holds. Otherwise ω^0_α and ω^0_β have to be calculated from the values θ_g and θ_I according to eqs 1−7 and taking $\phi_I = 0$.

Experimental Section

Cupric ions were introduced into MCM-41[16] and zeolite NaY (Union Carbide, LZY-52, $n_{Si}/n_{Al} = 2.5$) by liquid ion-exchange to produce Cu−MCM-41 and Cu−NaY. After dehydration the ion-exchanged samples were exposed to NC_5H_5 or NC_5D_5 at its room-temperature vapor pressure for 6 h. Cu−MCM-41 materials were loaded with $^{15}NC_5H_5$ or $^{15}NC_5D_5$, whereas samples Cu−NaY were exposed to $^{14}NC_5H_5$ or $^{14}NC_5D_5$. In the case of zeolite Cu−NaY, the loaded samples were heated to 353 K for 24 h to ensure complete complexation of the cupric ions by the pyridine molecules.

The formation of the tetrapyridine Cu(II) complex in the samples was checked by ESR spectroscopy at room temperature and at 77 K. The ESR spectra were recorded on a BRUKER ESP 300 spectrometer.

2D ESEEM experiments were performed on a BRUKER ESP 380 FT-ESR spectrometer at 4.2 K using the HYSCORE sequence ($\pi/2-\tau-\pi/2-t_1-\pi-t_2-\pi/2-\tau-$echo). Orientation selective HYSCORE spectra were measured at various spectral positions within the Cu(II) ESR powder patterns. Pulse lengths of 24 ns for $\pi/2$ pulses and 48 ns for π pulses were applied in the proton spectra. Pulse delays of $\tau = 32$ ns or $\tau = 40$ ns were chosen in the orientation selective 2D spectra to minimize blind spots in the HYSCORE powder pattern. The HYSCORE echo was detected via a remote echo sequence ($\pi/2-t_R-\pi/2-\tau_R-\pi-\tau_R-$echo)[23] as the dead time exceeds 32 ns in our experimental setup. The pulse delays of the remote echo sequence were $t_R = 4\ \mu$s and $\tau_R = 120$ ns. An eight-step phase cycle suggested by Gemperle et al.[27] was used to avoid interference with unwanted two- and three-pulse echoes. A 170 × 170 2D data matrix was sampled with a dwell time of 16 ns. In the deuterium spectra pulse lengths of 48 ns for $\pi/2$ pulses and 32 ns for π pulses were chosen to suppress diagonal peaks in the 2D spectra. The combination of relatively soft $\pi/2$ pulses and hard π pulses ensures an efficient exchange of the nuclear coherences between the two different M_S states by the mixing pulse. This is a necessary condition for the observation of cross-peaks in the 2D four-pulse experiment and especially critical for low-frequency nuclear transitions. Pulse delays of $\tau = 224$ ns or $\tau = 272$ ns were used to enhance deuterium modulation. Likewise, a 170 × 170 2D data matrix was sampled using the eight-step phase cycle. The dwell time was 64 ns. The echo decay was eliminated by a third-order polynomial baseline correction of the experimental data set in both time domains. 2D FT magnitude spectra were calculated and presented as contour plots.

Results

ESR. The ESR spectra at 77 K of the copper pyridine complex in the samples Cu−NaY and Cu−MCM-41 are illustrated in Figure 2. Both spectra can be described by axially symmetric Cu(II) **g** and $\mathbf{A}^{Cu}$ tensors. Room-temperature measurements gave comparable Cu(II) ESR spectra with slightly different parameters (not shown). This suggests that the complexes in both materials do not undergo reorientation processes at room temperature. The spin Hamiltonian param-

TABLE 1: ESR Parameters at 77 K and Room Temperature for Copper Pyridine Complexes in Samples Cu−NaY and Cu−MCM-41

sample	T (K)	$g_{\|}$[c]	$g_{\perp}$[c]	$A_{\|}^{63Cu}$[d] (cm^{-1})	$A_{\perp}^{63Cu}$[e] (cm^{-1})	$A_{\|}^{65Cu}$[d] (cm^{-1})	$A_{\perp}^{65Cu}$[e] (cm^{-1})	$A_{\perp}^{N}$[f] (cm^{-1})
Cu−NaY[a]	77	2.225	2.05	0.0196	0.0024	0.0210	0.0026	0.0016
	297	2.253	2.05	0.0185	0.0024	0.0198	0.0026	0.0015
Cu−MCM-41[b]	77	2.275	2.06	0.0180	0.0013	0.0192	0.0014	0.0017
	297	2.294	2.05	0.0169	0.0013	0.0180	0.0012	

[a] The line width in the simulation was $\Delta B_{\|} = 8$ G, $\Delta B_{\perp} = 12$ G. [b] The line width in the simulation was $\Delta B_{\|} = 30$ G, $\Delta B_{\perp} = 40$ G. ΔB is the peak-to-peak line width in the first-derivative spectrum. [c] Estimated error is ±0.003. [d] Estimated error for Cu−NaY is ±0.0004 cm^{-1} and for Cu−MCM-41 is ±0.0006 cm^{-1}. [e] Estimated error for Cu−NaY is ±0.0002 cm^{-1} and for Cu−MCM-41 is ±0.0004 cm^{-1}. [f] Note that $A_{\perp}^{N}$ refers to ^{14}N super hf coupling for Cu−NaY and ^{15}N hf coupling for Cu−MCM-41. Estimated errors are ±0.0001 cm^{-1} for Cu−NaY and ±0.0002 cm^{-1} for Cu−MCM-41. No nitrogen super hf coupling could be resolved for Cu−MCM-41 at $T = 297$ K.

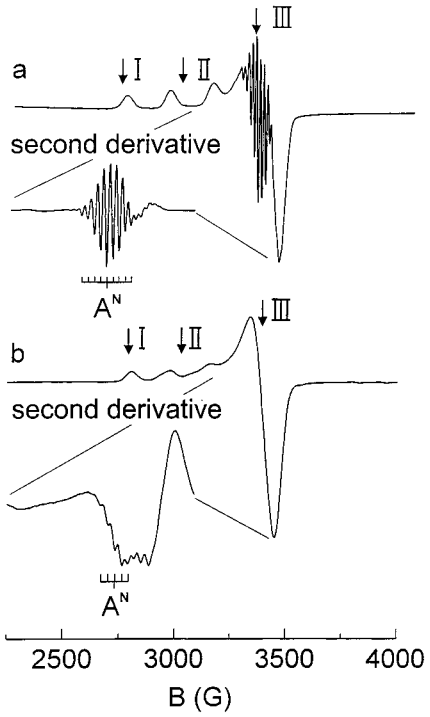

Figure 2. ESR spectrum of the copper pyridine complex at 77 K: (a) Cu−NaY and (b) Cu−MCM-41. Note that the sample Cu−NaY was loaded with $^{14}NC_5H_5$, whereas $^{15}NC_5H_5$ was used for Cu−MCM-41. The arrows indicate the spectral positions I, II and III, where orientation selective ESEEM spectra were measured.

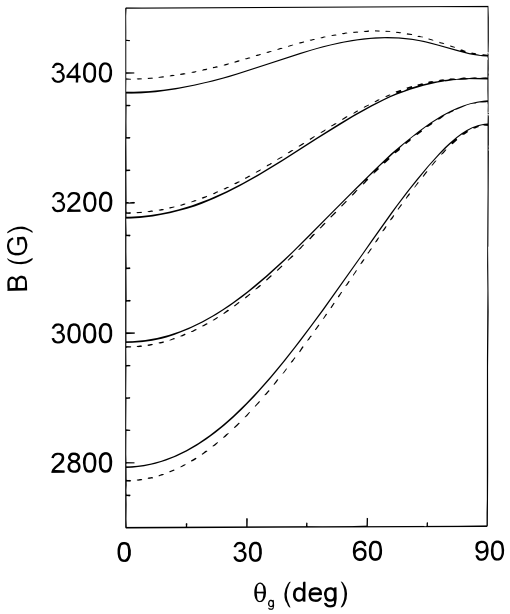

Figure 3. Calculated Cu(II) resonance fields dependent on the angle θ_g for the tetrapyridine copper(II) complex in Cu−NaY. Solid and dashed lines differentiate between the angular dependencies of the ^{63}Cu and ^{65}Cu isotopes.

eters of the copper pyridine complexes are summarized in Table 1. The parameters were determined by a simulation of the experimental ESR powder patterns using second-order perturbation theory. The hf interactions A^{63Cu} and A^{65Cu} of both copper isotopes ^{63}Cu (natural abundance 69.1%) and ^{65}Cu (natural abundance 30.9%) having a nucleus spin $I = {}^3/_2$ have been included in the simulation procedures as we cannot exclude a priori any impact of the weak ^{65}Cu hf signals in the ESR powder pattern on the orientation selective HYSCORE spectra. This point will be discussed in more detail in the following section. The spectrum of Cu−NaY loaded with $^{14}NC_5H_5$ shows a well-resolved superhyperfine (shf) splitting into nine lines at the $g_{\perp}$ spectral region of the Cu(II) powder pattern (Figure 2a). The number of shf lines suggests four equivalent nitrogen nuclei interacting with the unpaired electron. No nitrogen shf splitting was resolved at the $g_{\|}$ position in the experimental spectra. The simulations gave a rough estimate for $A_{\|}^{N}$ of the order of about (9×10^{-4}) cm^{-1} based on a comparison of the simulated powder patterns with the experimental line width and line shape near the $g_{\|}$ position.

The ESR spectrum of the copper pyridine complex in Cu−MCM-41 shows a much lower resolution than that of the sample Cu−NaY (Figure 2b). This is reflected in the significantly larger line widths, which were required in the simulations for Cu−MCM-41 (Table 1). Therefore, $^{15}NC_5H_5$ was adsorbed onto Cu−MCM-41 to improve the resolution of the nitrogen shf signals. In such samples five nitrogen shf signals were observed in the second-derivative spectrum indicating likewise an interaction of the unpaired electron with four equivalent nitrogen nuclei. The Cu(II) $g_{\|}$ and $A_{\|}^{Cu}$ parameters together with the nitrogen shf splitting are indicative for a coordination of the cupric ion to four pyridine ligands in a square planar coordination geometry.[8,9,12−14] Consequently, copper pyridine complexes exist in the form of $[Cu(NC_5H_5)_4]^{2+}$ in both materials.

It is useful to calculate the ESR resonance positions in dependence of the angle θ_g between the external magnetic field and the $g_{\|}$ axis of the Cu(II) **g** tensor to select proper field positions within the ESR powder pattern for the orientation selective HYSCORE measurements. As an example such a θ_g versus field plot is illustrated in Figure 3 for the $[Cu(NC_5H_5)_4]^{2+}$ complex in Cu−NaY. The presented angular dependence was calculated for both copper isotopes using second-order perturbation theory. The nitrogen shf splitting was omitted for clarification although it gives rise to a smearing of the resonance positions in the powder patterns.

HYSCORE Experiments on Cu−NaY. HYSCORE spectra of the $[Cu(NC_5H_5)_4]^{2+}$ complex were taken at three different field positions I (2793 G), II (3013 G), and III (3356 G) within the Cu(II) ESR powder spectrum (Figure 2). At these field

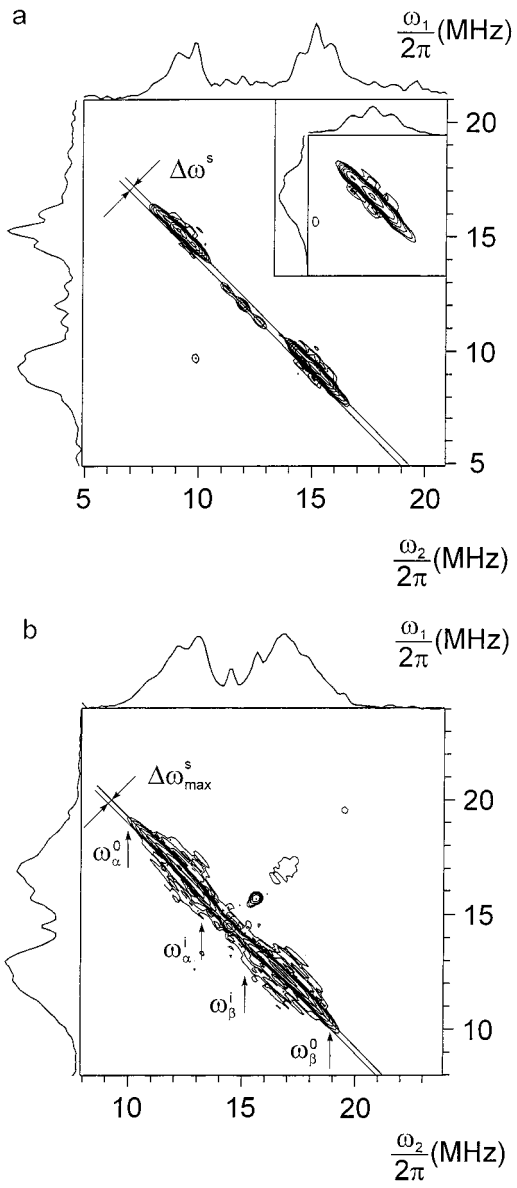

Figure 4. Experimental proton HYSCORE spectra of a $[Cu(NC_5H_5)_4]^{2+}$ complex in Cu−NaY. The spectra were recorded at the spectral positions (a) I (2793 G) and (b) III (3356 G). The maximum vertical shift $\Delta\omega^S_{max}/2\pi$ of the cross-peak ridges from the $\omega_1 = -\omega_2$ axis is illustrated by a solid line. The inner and outer end positions of the ridges $(\omega^i_{\alpha/\beta},\omega^i_{\beta/\alpha})$ and $(\omega^0_{\alpha/\beta},\omega^0_{\beta/\alpha})$ are marked by arrows. The insert shows an enlarged plot of the proton cross-peak showing the triplet structure.

positions crystallites with Cu(II) **g** tensors contribute to the ESR powder pattern whose $g_{||}$ axes form an angle $\theta_g = 0$, $\theta_g = 45°$, or $\theta_g = 90°$ with the external magnetic field (Figure 3). The orientations with $\theta_g = 0$ and $\theta_g = 90°$ correspond to the $g_{||}$ and $g_\perp$ spectral positions (Figure 1). Though a broad range of tensor orientations between $50° < \theta_g < 90°$ contribute to the spectrum taken at the spectral position III, we will refer in the following this position as the $g_\perp$ position. The proton spectra recorded at position III (Figure 4b) and position II (not shown) display two pronounced cross-peak ridges that are almost directed parallel to the off-frequency diagonal axes $\omega_1 = -\omega_2$, indicating protons with substantial dipolar hyperfine coupling. The small shift of the ridges from the $\omega_1 = -\omega_2$ axis toward higher frequencies is likewise caused by the dipolar part $T_\perp$ of the proton hyperfine coupling.[23,24] We determine comparable value $\Delta\omega^S_{max}/2\pi = 0.22$ MHz (Figure 4b) for the maximum shift of the ridges from the $\omega_1 = -\omega_2$ axis. A dipolar hf coupling parameter $T_\perp = 2.8$ MHz for these strongly coupled protons is estimated from $\Delta\omega^S_{max}$ according to eq 8. From the inner end position of the ridges at (13.3, 15.3) MHz and (15.3, 13.3) MHz (Figure 4b), we deduce an isotropic proton hf coupling $A_{iso} = 4.8$ MHz substituting $T_\perp = 2.8$ MHz into eq 9. On the basis of previous results,[24,26] we assign these hf parameters to the two H2 and H6 protons of the pyridine ligand molecules with a Cu(II)− H distance of about 3.1 Å (Figure 1). Of course, the accuracy in the determined value A_{iso} is low (±0.2 MHz) as the ridges are overlapped in the spectral region near the proton nuclear Larmor frequency ω_I at (14.29, 14.29) MHz (Figure 4b) by signals from weakly coupled protons. This might be protons of uncoordinated pyridine molecules or protons in H3/H5 and H4 positions of pyridine ligand molecules. The cross-peak ridges of the protons H2 and H6 approach the $\omega_1 = -\omega_2$ axis at their outer end positions $(\omega^0_\alpha,\omega^0_\beta)$ and $(\omega^0_\beta,\omega^0_\alpha)$. These part of the HYSCORE powder pattern corresponds to crystallite orientations where the external magnetic field is almost aligned along the *z* axis of the proton hf tensor.[24] This axis corresponds to the largest principal value A^p_{zz} of the proton hf coupling tensor $\mathbf{A^P}$. A comparison between the spectra taken at the position III (Figure 4b) and II (not shown) indicates that $(\omega^0_\beta - \omega^0_\alpha)$ is by 0.3 MHz larger for irradiation at the spectral position II ($\theta_g = 45°$). We determine $\omega^0_\alpha = 7.6$ MHz and $\omega^0_\beta = 18.0$ MHz for the spectrum that was measured at the spectral position II. The spectrum taken at the spectral position I corresponding to the $g_{||}$ position (Figure 4a) displays two more groups of cross-peaks besides the peak of weakly coupled protons at the nuclear Larmor frequency (11.93, 11.93) MHz. The ridge-type shape of these cross-peaks is not as pronounced as those observed in the spectra that were measured at the $g_\perp$ position and at the intermediate position at $B = 3013$ G. This is a direct consequence of the orientation selective ESEEM experiment for irradiation near the $g_{||}$ position of the Cu(II) ESR powder pattern. Only those complexes are selected whose $g_{||}$ axis is approximately directed parallel to the external magnetic field ($\theta_g = 0$). The peaks at (9.03, 15.15) MHz and at (15.14, 9.03) MHz are suggestive of protons with strong hf couplings. They are likewise assigned to the H2 and H6 protons of the pyridine ligand molecules. A close inspection of the ridges reveal that they are composed of triplets with an approximate intensity ratio of 1:2:1. This might indicate that protons H2/H6 with different hf coupling parameters or with slightly different hf tensor orientations contribute to those cross-peaks. The cross-peaks of proton H2/H6 peaks are shifted by $\Delta\omega^S = 0.25$ MHz from the $\omega_1 = -\omega_2$ axis toward higher frequencies indicating a substantial effect of the second-order dipolar coupling parameter *B* on the proton nuclear transition frequencies. We determine $B/2\pi = 4.11$ MHz using the relation[24]

$$B = [(8\Delta\omega^S\omega_I)/(2^{1/2})]^{1/2} \qquad (11)$$

The other cross-peaks at (11.23, 12.7) MHz and (12.7, 11.23) MHz are not significantly shifted from the $\omega_1 = -\omega_2$ axis. This suggests that they are caused by protons with comparable small dipolar hf couplings such as protons H3, H4, and H5 of pyridine ligands or distant protons of uncoordinated pyridine molecules.

An orientation selective deuterium HYSCORE spectrum of the $[Cu(NC_5D_5)_4]^{2+}$ complex in Cu−NaY measured at the $g_{||}$ position (spectral position I) is illustrated in Figure 5. The spectrum shows cross-peak ridges from deuteriums with substantial hf couplings that are split by the nq interaction. As

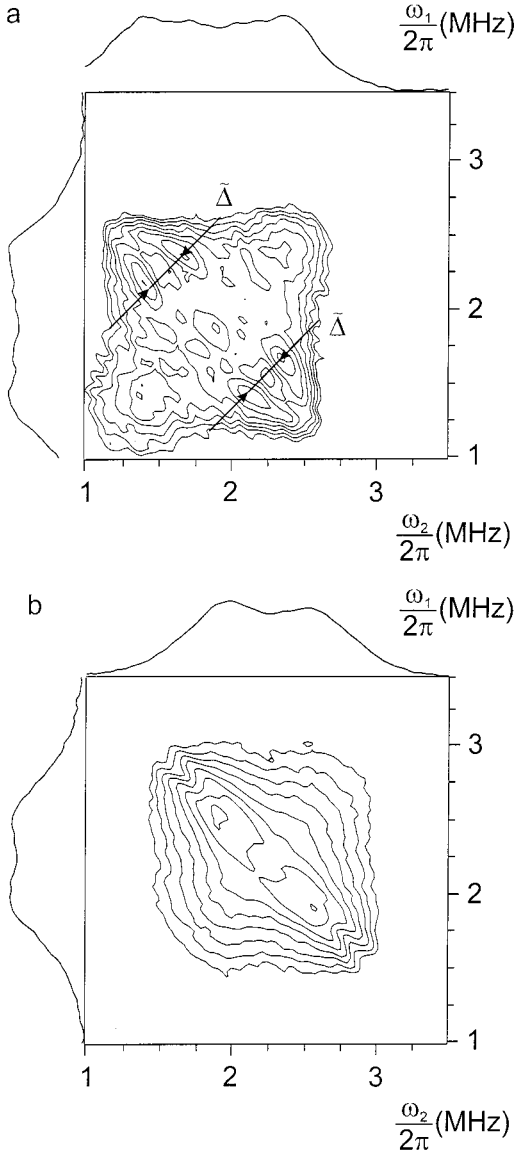

Figure 5. Experimental deuterium HYSCORE spectra of a $[Cu(NC_5D_5)_4]^{2+}$ complex in Cu−NaY measured at the spectral position I (2793 G). The arrows show the mean nq splitting $\tilde{\Delta}$ of the ridges.

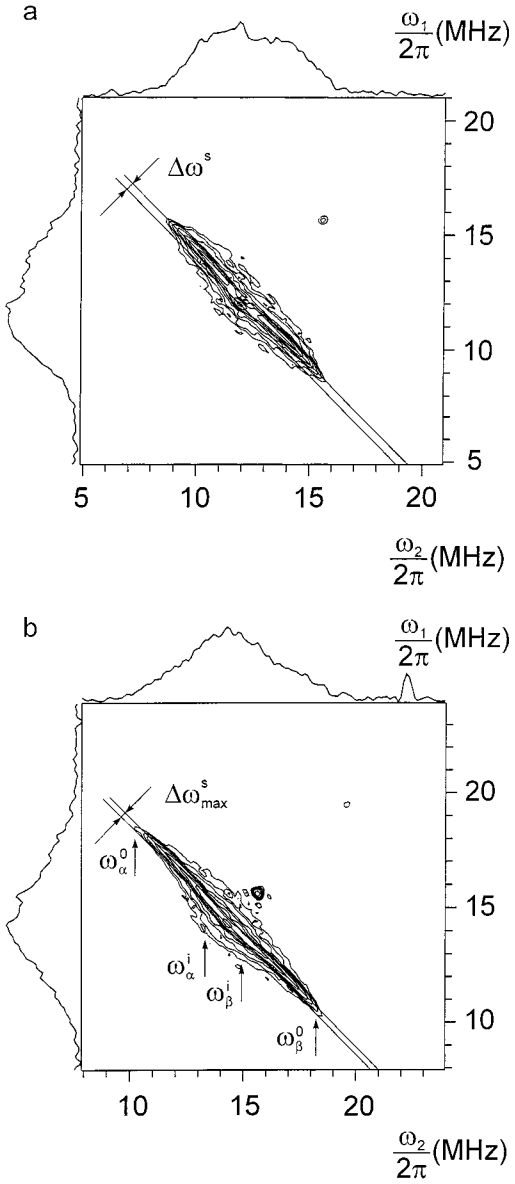

Figure 6. Experimental proton HYSCORE spectra of a $[Cu(NC_5H_5)_4]^{2+}$ complex in Cu−MCM-41. The spectra were recorded at the spectral positions (a) I (2800 G) and (b) III (3396 G). The maximum vertical shift $\Delta\omega^S_{max}/2\pi$ of the cross-peak ridges from the $\omega_1 = -\omega_2$ axis is illustrated by a solid line. The inner and outer end positions of the ridges $(\omega^i_{\alpha/\beta},\omega^i_{\beta/\alpha})$ and $(\omega^0_{\alpha/\beta},\omega^0_{\beta/\alpha})$ are marked by arrows.

already discussed for the proton case the ridge-type shape of these cross-peaks is not as pronounced as those observed in the spectra that were measured at the $g_\perp$ position. The mean positions (1.4, 2.3) MHz and (2.3, 1.4) MHz of the deuterium cross-peak ridges are comparable to those of the cross-peaks of the protons H2 and H6 of the pyridine ligands in the $g_{||}$ spectrum of the $[Cu(NC_5H_5)_4]^{2+}$ complex regarding the ratio between the proton and the deuterium nuclear Larmor frequency. However, a triplet structure of the cross-peaks could not be observed as in the proton spectrum owing to the poor spectral resolution of the deuterium HYSCORE spectrum. Otherwise, the nq splitting of the ridges measured along the $\omega_1 = -\omega_2$ axis varies between $\Delta_{min}/2\pi\sqrt{2} = 0.07$ MHz and $\Delta_{max}/2\pi\sqrt{2} = 0.24$ MHz with a mean value $\tilde{\Delta}/2\pi\sqrt{2} = 0.18$ MHz. This suggests that deuterium nuclei with different orientations of their nq tensors with respect to the Cu(II) **g** tensor contribute to the observed cross-peaks.

The broad features at the frequency diagonal axis $\omega_1 = \omega_2$ are diagonal peaks. They result from an insufficient mixing of the π pulse between the two evolution periods t_1 and t_2 in the HYSCORE experiment.[27]

HYSCORE Experiments on Cu−MCM-41. HYSCORE spectra of the $[Cu(NC_5H_5)_4]^{2+}$ complex are illustrated in Figure 6. The spectra were measured at three different field positions I (2800 G), II (3013 G), and III (3396 G) within the Cu(II) ESR powder spectrum corresponding to crystallite orientations $\theta_g = 0$ ($g_{||}$ position), $\theta_g = 45°$, or $\theta_g = 90°$ ($g_\perp$). Extended cross-peak ridges of the protons H2 and H6 from coordinated pyridine molecules were again observed in the spectrum taken at the spectral positions III (Figure 6b) and II (not shown). We determine a comparable dipolar hf coupling parameter $T_\perp = 2.6$ MHz from the maximum shift of the cross-peaks $\omega^S_{max}/2\pi = 0.20$ MHz from the $\omega_1 = -\omega_2$ axis (Figure 6b). An isotropic proton hf coupling $A_{iso} = 4.1$ MHz is estimated from the inner end positions of the ridges at (13.5, 15.0) MHz and (15.0, 13.5) MHz. However, this spectral region is again overlapped by signals from weakly coupled protons. The maximum extension of the ridges $(\omega^0_\beta - \omega^0_\alpha)$ is now observed in the spectrum

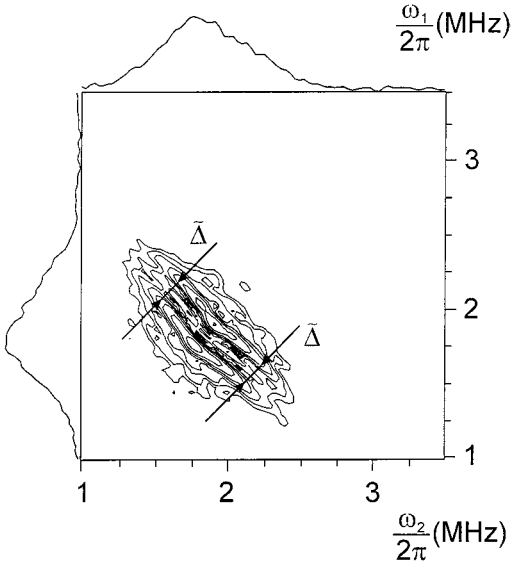

Figure 7. Experimental deuterium HYSCORE spectra of a $[Cu(NC_5D_5)_4]^{2+}$ complex in Cu−MCM-41 measured at the spectral position (a) I (2800 G). The arrows show the mean nq splitting $\tilde{\Delta}$ of the ridges.

measured at the $g_\perp$ position (position III), whereas in samples Cu−NaY spectra taken at the intermediate field position II provided a maximum extension of the cross-peak ridges. A close inspection of the outer end positions gives $\omega_\alpha^0 = 9.6$ MHz and $\omega_\beta^0 = 18.9$ MHz. In contrast to the sample Cu−NaY the HYSCORE spectrum of the $[Cu(NC_5H_5)_4]^{2+}$ complex in Cu−MCM-41 recorded at the $g_{||}$ position (field position I) of the Cu(II) ESR powder pattern also displays extended cross-peak ridges (Figure 6a), which we assign to the protons H2/H6 of the pyridine ligands. The shift $\Delta\omega^S = 0.23$ MHz of the ridges from the $\omega_1 = -\omega_2$ axis suggests again a substantial effect of the second-order dipolar coupling parameter B on the nuclear transition frequencies of the protons H2 and H6. The occurrence of such elongated ridges in the single-crystal type ESEEM spectrum at the $g_{||}$ indicates a strong disorder in the ligand arrangement in the tetrapyridine copper(II) complex.[25]

The HYSCORE spectrum of the $[Cu(NC_5D_5)_4]^{2+}$ complex in Cu−MCM-41 recorded at the $g_{||}$ position (position I) exhibits well-resolved deuterium cross-peak ridges with the typical splitting of the ridges due to the deuterium nq interaction (Figure 7). The observed ridges are likewise assigned to the D2/D6 deuteriums of coordinated pyridine molecules on the basis of a comparison with the cross-peak ridges from protons H2/H6 in Figure 6. The nq splitting of the ridges has a mean value of about $\tilde{\Delta}/2\pi\sqrt{2} = 0.06$ MHz, which is smaller than the value estimated from the deuterium spectrum of the $[Cu(NC_5D_5)_4]^{2+}$ complex in Cu−NaY. Furthermore, the nq splitting does not significantly vary along the ridges. This is again in contrast to the results on the sample Cu−NaY and points at different orientations of the deuterium nq tensors with respect to the Cu(II) **g** tensor in both materials.

Discussion

The ESR results show that tetrapyridine copper(II) complexes are formed in both materials Cu−NaY and Cu−MCM-41 upon adsorption of pyridine. The Cu(II) spin Hamiltonian parameters do not significantly change in the range between 77 K and room temperature indicating the absence of fast reorientation processes of the complexes. This suggests that the complexes are restricted in their mobility by the interaction with the host lattice. The small differences in the Cu(II) parameters between 77 K and room temperature are presumably caused by Cu−N bond vibrations within the complexes as discussed by Vedrine el al.[13]

The Cu(II) spin Hamiltonian parameters of the copper pyridine complex determined from the ESR spectra are indicative for a square planar coordination of the cupric ion to four nitrogens.[11−14,16] However, they do not allow to deduce the overall complex geometry such as the arrangement of the pyridine ligand molecules with respect to the Cu(II) **g** tensor. For instance, the pyridine ligand molecules of the tetrapyridine copper (II) complex have two degrees of disorder as shown in a previous investigation of the $Cu(NC_5H_5)_4]^{2+}$ complex in frozen solution. One is described by a tilt of the Cu−N bond out of the complex plane with the angle ϵ_1 and the other by a rotation around the Cu−N bond indicated by the angle ϵ_2 in Figure 1. This information can be gained by a detailed analysis of the orientation selective HYSCORE spectra[25] as shown below.

Cu−NaY. The orientation of the pyridine ligands were derived from the HYSCORE spectrum measured at the $g_{||}$ position using the parameter $B/2\pi = 4.11$ MHz and the estimated hf dipolar coupling parameter $T_\perp = 2.8$ MHz of the protons H2 and H6 in the pyridine ligands of the tetrapyridine copper(II) complex. For irradiation at the $g_{||}$ position

$$B = 2\pi T_\perp 3 \cos\theta_I \sin\theta_I \qquad (12)$$

holds according to eqs 3−7. The determined value $\theta_I = 46°$ suggests that the pyridine ligand molecules are orientated with their molecular plane perpendicular to the complex plane (ligand molecule I in Figure 1, $\epsilon_2 = 90°$). For this case we can calculate from the known geometry of the pyridine molecule and an assumed Cu−N distance of 2.1 Å an angle $\theta_I = 47°$ in good agreement with the estimated value for θ_I. The fact that the maximum extension of the cross-peak ridges of protons H2/H6 was observed in the spectrum measured at the spectral position II, where the angle $\theta_g = 45°$ was selected, supports this interpretation. We likewise determine $\theta_I = 45°$ from $\omega_\alpha^0 = 7.6$ MHz, $\omega_\beta^0 = 18.0$ MHz, and the values obtained for $T_\perp$ and A_{iso}. Comparable orientations of ligand molecules, where the pyridine molecules are arranged with their molecular plane perpendicular to the complex plane, have been found for tetrapyridine copper(II) complexes in frozen solution.[25]

The deuterium HYSCORE spectrum taken at the $g_{||}$ position supports the result derived from the proton HYSCORE spectra. If we neglect possible differences in the orientation of the quantization axis of the nucleus spin in the two M_S manifolds in a first approximation, we can estimate the angle θ_Q between the z axis of the deuterium nq tensor and the external magnetic field from the nq splitting $\Delta/\sqrt{2}$ of the cross-peak ridges in the 2D spectra according to

$$\frac{\Delta}{2\pi\sqrt{2}} \approx \frac{3Q_{zz}}{2}(3\cos^2\theta_Q - 1) \qquad (13)$$

The principal values of the deuterium nq tensor in pyridine are $|Q_{zz}| = 0.090$ MHz and $|Q_{xx}| = |Q_{yy}| = 0.045$ MHz where the z axis of **Q** points along the D2−C2 bond.[29] Taking the mean value $\tilde{\Delta}/2\pi\sqrt{2} = 0.18$ MHz for the nq splitting of the deuterium cross-peak ridges we determine $\theta_Q = 28°$. We calculate an angle of 30° for pyridine ligand molecules of type I (Figure 1) on the basis of the geometry of the pyridine molecule in good accordance with the experimentally obtained value for θ_Q.

Up until now, we have not discussed the origin of the triplet structure of the proton cross-peaks observed in the HYSCORE spectrum measured at the $g_{||}$ position. We have to discuss two

experimental situations that might cause such triplets. One is related to the superposition of the ESR powder patterns of the ^{63}Cu and ^{65}Cu isotopes. It is obvious from the θ_g versus field plot in Figure 3 that we have a superposition of two different crystallite orientations if we select a field position that corresponds to the $g_{||}$ position of the ^{63}Cu ESR spectrum. Whereas crystallites with $\theta_g \approx 0$ from the ^{63}Cu ESR spectrum contribute to the HYSCORE spectrum, the ^{65}Cu ESR spectrum is irradiated at a position corresponding to **g** tensor orientations with $\theta_g \approx 12°$. Otherwise, small distortions in the ligand arrangement may also cause a splitting of the cross-peaks into triplets as observed at the $g_{||}$ position. A tilt of the pyridine ligands out of the Cu−N_4 complex plane by $\epsilon_1 = 11°$ would result in angles $\theta_I = 58°$ for proton H2 and $\theta_I = 36°$ for proton H6, which in turn would give rise to the two outer components of the triplet. The central component is then due to the pyridine ligands with $\epsilon_1 = 0°$, which are exactly perpendicular with their molecular plane to the complex plane. The 1:2:1 intensity ratio of the triplet suggests that one out of two ligand molecule of type I is tilted by $\epsilon_1 = 11°$ out of the Cu−N_4 complex plane.

Spectral simulations were performed to decide between the two sources for the triplet splitting. In the simulations a proton hf coupling tensor $A^p_{zz} = 10.4$ MHz, $A^p_{xx} = A^p_{yy} = 2.0$ MHz calculated from the experimentally obtained values for A_{iso} and $T_\perp$ was used. Figure 8a illustrates a proton HYSCORE spectrum, which was simulated for a case where different **g** tensor orientations of both copper isotopes contribute to the spectrum. The spectrum was calculated by a superposition of two HYSCORE spectra with $\theta_g = 1°$ and $\theta_g = 12°$

$$\langle E_{mod}\rangle = \langle E_{mod}(\theta_g = 1°)\rangle + \frac{I^{ESR}(^{65}\text{Cu}, \theta_g = 12°)}{I^{ESR}(^{63}\text{Cu}, \theta_g = 0)}\langle E_{mod}(\theta_g = 12°)\rangle \quad (14)$$

where the expression for the four-pulse ESEEM modulation

$$\langle E_{mod}(\theta_g)\rangle = C\int_{-\Delta\epsilon_1}^{\Delta\epsilon_1}\int_0^{\pi} E_{mod}(\theta_g, \phi, \epsilon_1)\, F(\epsilon_1, \Delta_1)\, d\phi\, d\epsilon_1 \quad (15)$$

was computed by the procedure discussed in a previous paper.[25] The quantity C in eq 15 is a normalization factor. In the simulation a small variance $\Delta\epsilon_1 = 1°$ in ϵ_1 with a Gaussian weighting function $F(\epsilon_1, \Delta_1 = 1°)$ was used. The intensity ratio

$$\frac{I^{ESR}(^{65}\text{Cu}, \theta_g = 12°)}{I^{ESR}(^{63}\text{Cu}, \theta_g \approx 0)} \leq 1$$

between the ^{63}Cu and ^{65}Cu ESR spectra was estimated by simulations of the ESR powder spectra of both copper isotopes, where the experimental line width and the natural abundance of the isotopes was taken into account. Whereas the spectrum at $\theta_g = 1°$ resulting from the ESR spectrum of the ^{63}Cu isotope provides a single-crystal type cross-peak spectrum, the simulation performed for $\theta_g = 12°$ (^{65}Cu isotope) gives cross-peaks with a double-peak structure (see inset in Figure 8a). These features are well-known from orientation-selective ENDOR experiments.[30] However, on the basis of our simulations (Figure 8a), the intensity of the double-peak structure is not sufficient to provide together with the $\theta_g = 1°$ spectrum a cross-peak triplet with an approximate 1:2:1 intensity ratio. A much better agreement between experiment and simulation was obtained for the second assumption. Figure 8b illustrates a spectrum that was calculated for a superposition of signals from protons with angles $\theta_I = 47°$, $\theta_I = 58°$, and $\theta_I = 36°$ corresponding to

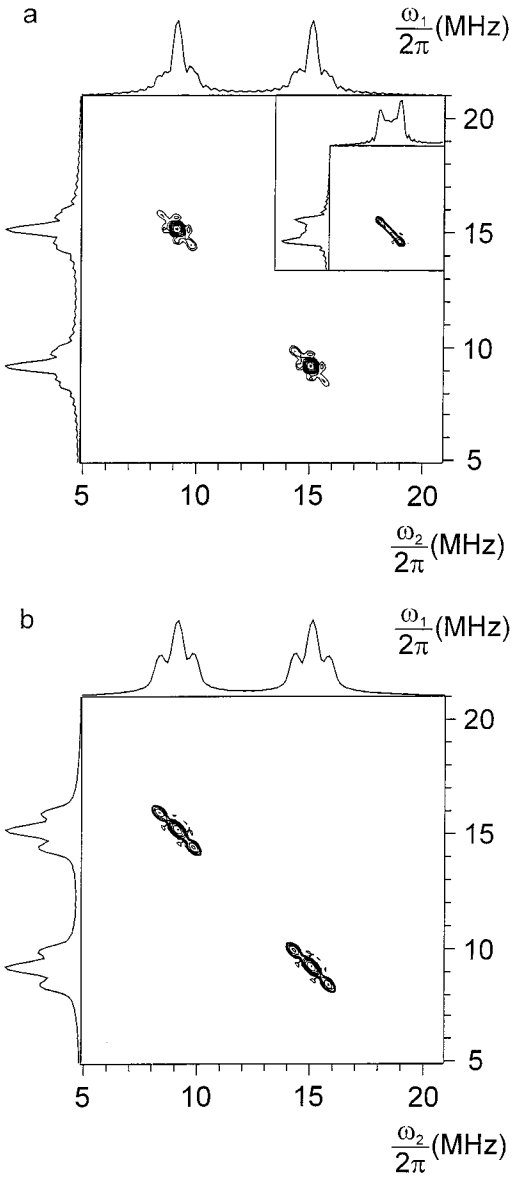

Figure 8. Simulated proton HYSCORE spectra of pyridine ligand molecule I for an axially symmetric **g** tensor and microwave irradiation near the $g_{||}$ ($\theta_g = 0$) position: (a) Superposition of spectra from both copper isotopes with $\theta_g = 1°$ (^{63}Cu) and $\theta_g = 12°$ (^{65}Cu), $\Delta\epsilon_1 = 1°$. The insert shows the cross-peak shape for the $\theta_g = 12°$ spectrum alone. (b) Superposition of three different proton spectra for $\theta_I = 47°$, $\theta_I = 58°$, and $\theta_I = 36°$, $\Delta\epsilon_1 = 4°$.

orientations of the pyridine molecule I with $\epsilon_1 = 0$ and $\epsilon_1 = 11°$. The intensity ratio between the $\epsilon_1 = 0$ and $\epsilon_1 = 11°$ spectra was assumed to be 2:1, and $\theta_g = 1°$ was fixed in the simulation. For all three spectra a small variance $\Delta\epsilon_1 = 4°$ in the Cu−N bond direction was assumed to account for the experimental line width of the triplet constituents.

The deuterium HYSCORE spectrum measured at the $g_{||}$ position supports the assumption that the triplet structure of the proton cross-peaks is not caused by the superposition of the ESR powder patterns of the ^{63}Cu and ^{65}Cu isotopes but is due to slightly different arrangements of the ligand molecules. For comparison deuterium HYSCORE spectra were calculated for both cases (Figure 9). In the simulations a deuterium hf tensor $A^D_{zz} = 1.59$ MHz, $A^D_{xx} = A^D_{yy} = 0.31$ MHz determined from the proton data of the $[Cu(NC_5H_5)_4]^{2+}$ complex in Cu−NaY and a deuterium nq tensor $|Q_{zz}| = 0.090$ MHz, $|Q_{xx}| = |Q_{yy}| = 0.045$ MHz were used where the z axis of the deuterium **Q** tensor

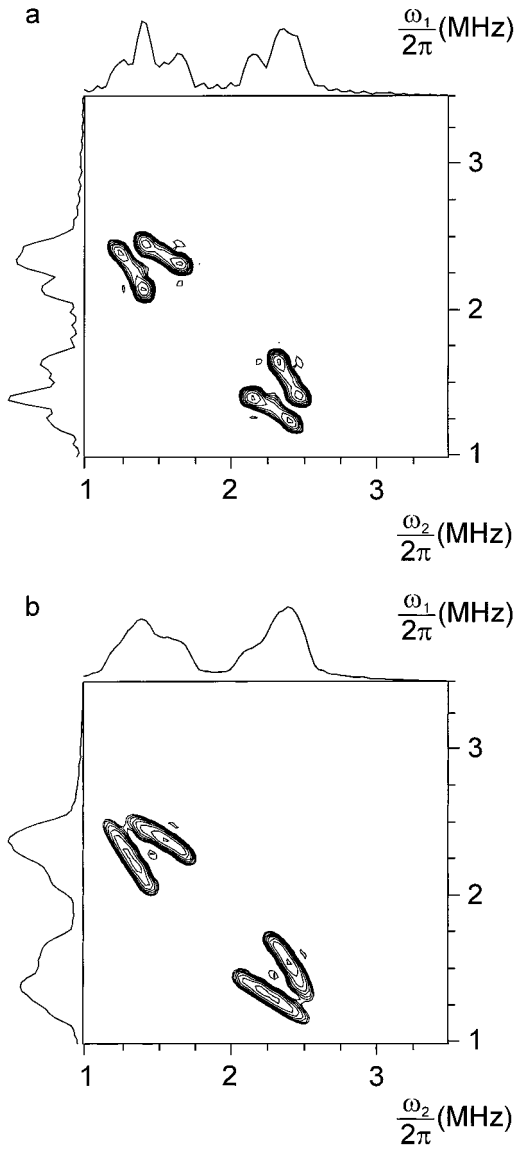

Figure 9. Simulated deuterium HYSCORE spectra of pyridine ligand molecule I for an axially symmetric **g** tensor and microwave irradiation at different spectral position within the ESR powder pattern: (a) $\theta_g = 12°$ with $\Delta\epsilon_1 = 1°$, and (b) $\theta_g = 1°$ ($g_{||}$ position), $\Delta\epsilon_1 = 12°$, where a superposition of three different deuterium spectra with $\theta_I = 47°$, $\theta_I = 58°$, and $\theta_I = 36°$ was calculated.

was again assumed to point along the D2−C2 bond.[25] We have to stress that the triplet structure was not resolved in the experimental deuterium HYSCORE spectrum. Therefore, a larger variance $\Delta\epsilon_1 = 12°$ in the Cu−N bond directions was used in the simulation of the spectrum displayed in Figure 9b. Only the spectrum for $\theta_g = 12°$, which arises from the ^{65}Cu isotope, was calculated in the deuterium case to show the effect of an insufficient orientation selection in the deuterium 2D ESEEM spectra. A comparison between the simulated spectra in Figure 9 with the experimental one in Figure 5a shows that the simulated spectrum for irradiation at $\theta_g = 12°$ does not reproduce the observed curvature of the deuterium cross-peak ridges. Therefore, we conclude the cross-peak shapes in the proton and deuterium HYSCORE spectra measured at the $g_{||}$ spectral position are caused by small tilts of the Cu−N bond directions of the pyridine ligands out of the Cu−N_4 complex plane. Such variations has been also observed for tetrapyridine copper(II) complexes in frozen solution, where they were much more pronounced.[25]

Although the HYSCORE spectra measured at the $g_{||}$ spectral position give very detailed information about pyridine ligand molecules of type I, they fail to provide reliable results about type II molecules. As these molecules are with their molecular plane within the mean complex plane, the magnetic field direction is close to the A_{xx} or A_{yy} principal axis of the hf coupling tensors of the protons H2/H6 or the corresponding deuteriums for irradiation at the $g_{||}$ spectral position. Consequently, small modulation intensities have to be expected for proton and deuterium nuclei from type II ligand molecules. Otherwise, nuclei from type II ligands should give rise to intense cross-peak ridges in spectra taken near the $g_{||}$ spectral position.[24] Therefore, proton HYSCORE spectra for irradiation at the $g_\perp$ spectral position were simulated and compared with the experimental spectrum to estimate in particular the relative number of ligand molecules of type I and II. The spectra have been simulated using the expression

$$\langle E_{mod}\rangle = C\int_0^{\pi}\int_{\theta_g=50°}^{\theta_g=90°} E_{mod}(\theta_g, \phi)\sin\theta_g\, d\theta_g\, d\phi \quad (16)$$

where C is again a normalization factor. The integration over θ_g takes care that a broad range of crystallite orientations contribute to the ESR spectrum at the spectral position III (Figure 3). The small disorder in ϵ_1 has been omitted to save computing time as it has only a minor effect on the cross-peak shapes in the spectrum measured at the $g_\perp$ spectral position of the Cu(II) powder pattern. Exclusively simulations with ligand orientations such as molecule I gave a satisfactory accordance with the experimental spectra. Therefore, we may conclude that within our experimental accuracy all four pyridine ligand molecules in the tetrapyridine copper(II) complex in the sample Cu−NaY are oriented with their molecular plane perpendicular to the Cu−N_4 mean complex plane.

On the basis of the above arguments, we can now assign the low intense cross-peaks at (11.23, 12.7) MHz and (12.7, 11.23) MHz observed in the spectrum taken at the $g_{||}$ spectral position to the protons in the H3 and H5 positions of molecule I (Figure 1). These protons have a Cu(II)−H distance of 5.2 Å. This translates into a dipolar hf coupling parameter $T_\perp = 0.57$ MHz. The z axes of their hf interaction tensors form an angle of $\theta_I = 65°$ with the $g_{||}$ axis. We determine from the quantities $T_\perp$, θ_I and the cross-peak positions an isotropic hf coupling $A_{iso} = 1.7$ MHz for the protons H3/H5. This value compares to the isotropic hf couplings of 1.3−1.7 MHz of the protons in position 3 in copper-8-hydroxyquinolinate complexes incorporated in various host crystals.[31]

The results of the 2D ESEEM experiments show that variance in the ligand arrangement of the tetrapyridine copper(II) complex is considerably smaller than was found for the same complex in frozen solution with pyridine as solvent.[25] This indicates that in the Cu−NaY zeolite, where the maximum dimension of the $[Cu(NC_5H_5)_4]^{2+}$ complex of about 12 Å is approaching the diameter of the supercage (13 Å),[14] the interaction of the complex with the zeolite host becomes important and puts some structural constraints on the geometry of the complex. The determined coordination geometry of the complex seems to be a direct consequence of the interaction of the $[Cu(NC_5H_5)_4]^{2+}$ complex with the zeolite structure. Basically, the metal complex can be located at two possible sites in the Y zeolite structure, the center of the supercage or the center of the 12-membered rings. It seems justified to assume that the ligands are preferably arranged in such a way that their spatial constraints with the inner surface of the host material are minimized. This suggests that the metal ion of the tetrapyridine copper(II) complexes is

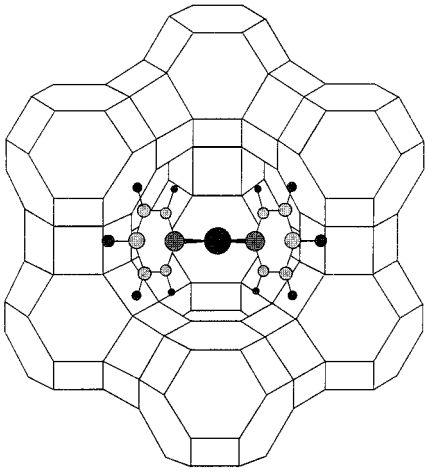

Figure 10. Possible site of the tetrapyridine copper(II) complex in Cu−NaY zeolite. The Cu(II) ion is located at the center of the 12-membered ring. Two of the four pyridine ligand molecules point into each neighboring supercage. Only the pyridine ligands in the front supercage are shown.

located at the center of the 12-membered rings, which connects two supercages in the Y zeolite structure. Two of the four coordinated pyridine molecules point into each of the neighboring supercages. The proposed model of the site of the tetrapyridine copper(II) complex in Cu−NaY zeolite is depicted in Figure 10. At this site, only such ligand molecules minimize their spatial constraints with the zeolite framework, which are aligned parallel with their molecular mirror plane to the four- or six-ring structures forming the walls of the supercages. Consequently, the pyridine ligands must be arranged with their molecular plane perpendicular to the $Cu-N_4$ complex plane in accordance with the Y zeolite structure and our analysis of the overall coordination geometry of the tetrapyridine copper (II) complex. Such an adsorbate strucuture of the pyridine ligands with respect to the zeolite surface might indicate the formation of a bonding between the ligand and the zeolite framework. The absence of motional effects in the ESR spectra of the $[Cu(NC_5H_5)_4]^{2+}$ complex also suggests a strong interaction of the complex with the inner surface of the zeolite, for instance due to a bonding of the ligands to the host lattice. Presumably, the observed small tilts of the Cu−N bond direction of two ligand molecules with respect to the $Cu-N_4$ mean complex plane of about 11° are also a result of the optimization of the geometry of the bonding between ligand and zeolite framework. A position of the $[Cu(NC_5H_5)_4]^{2+}$ complex at the center of the 12-membered rings is likewise reasonable from electrostatic arguments. Calculations of the electrostatic potential within the Y zeolite structure using electronegativity equalization methods[32] showed that a local potential minimum exists exactly at the center of the 12-ring structure, which might favor the location of the complexed cupric ion at this position. Finally, it seems worthwhile to note that the isotropic hf coupling $A_{iso} = 4.8$ MHz of the H2/H6 protons in the tetrapyridine Cu(II) complex in Cu−NaY is about 15% larger in comparison to those determined in a frozen pyridine solution.[25] This indicates a displacement of the spin density into the ligand system of the encapsulated complex. Such spin delocalizations over the ligands have already been discussed by Dai et al.[14] as an important factor in the stabilization of metal complexes in zeolites. The displacement of the spin density might be caused by the spatial distribution of the electrostatic potential within the supercage and gives a further indication on a strong interaction between the complex ligands and the zeolite host.

Cu−MCM-41. The determined hf coupling parameters $T_\perp = 2.6$ MHz and $A_{iso} = 4.1$ MHz of the protons H2/H6 of the tetrapyridine copper (II) complex in Cu−MCM-41 are in agreement with previously reported results, which were obtained by analysis of a single-proton HYSCORE spectrum measured at the $g_\perp$ spectral position of the Cu(II) ESR powder spectrum.[24] This is in agreement with the observation that the maximum extension of the ridges is observed in the spectrum taken at the spectral position III ($g_\perp$ position). Taking $\omega_\alpha^0 = 9.6$ MHz, $\omega_\beta^0 = 18.9$ MHz, $\theta_g = 90°$, $\phi_I = 0$ and the estimated values for $T_\perp$ and A_{iso}, we actually obtain $\theta_I = 90°$ according to eq 1. This suggests that the z axis of the proton hf coupling tensor is within the $g_\perp$ plane and pyridine ligand molecules are oriented parallel with their molecular plane to the complex plane as shown for molecules of type II in Figure 1. However, the pronounced ridges that were observed in the spectra measured at the $g_{||}$ spectral position indicate that a substantial number of ligand molecules have to deviate from this in-plane coordination. The orientation-selective HYSCORE experiments and in particular the deuterium spectra presented in this work enable us to determine the complex geometry in more detail. The cross-peak pattern in the deuterium spectrum of the $[Cu(NC_5D_5)_4]^{2+}$ complex in Cu−MCM-41 measured at the $g_{||}$ spectral position differs strongly from those of the deuterated complex in Cu−NaY. The nq splitting of the ridges $\tilde{\Delta}/2\pi\sqrt{2} = 0.06$ MHz is much smaller and almost constant along the ridges in the spectrum of the sample Cu−MCM-41. If we assume that the deuterium nq tensor is not significantly altered by the interaction of the complex with the inner surface of the MCM-41, the observed nq splitting suggests orientations of the external magnetic field that are almost perpendicular to the z axis of the deuterium nq tensor. This would correspond to orientations of the pyridine ligand where the molecular plane of the pyridine molecule is parallel to the $Cu-N_4$ mean complex plane ($\epsilon_1 = \epsilon_2 = 0$, molecule II in Figure 1). The observation of the maximum extension of the cross-peak ridges in the proton spectrum measured at the field position III ($g_\perp$ position) supports this conclusion. However, the pronounced ridges in the proton and deuterium spectra taken at the $g_{||}$ position indicate a substantial disorder in the ligand arrangement as shown by the simulation of the HYSCORE spectra. The main features of the cross-peak ridges in the proton and deuterium spectra taken at the $g_{||}$ position can fairly be reproduced in the spectral simulations if we assume a strong variance $\Delta\epsilon_1 = \Delta\epsilon_2 = 42°$ for the angles ϵ_1 and ϵ_2 (Figure 11). The spectra in Figure 11 were simulated using the expression

$$\langle E_{mod}\rangle = C \int_{-\Delta\epsilon_2}^{\Delta\epsilon_2}\int_{-\Delta\epsilon_1}^{\Delta\epsilon_1}\int_0^{\pi}\int_{\theta_g=50°}^{\theta_g=90°} E_{mod}(\theta_g, \phi, \epsilon_1, \epsilon_2) \times F(\epsilon_1, \Delta_1)\, F(\epsilon_2, \Delta_2) \sin\theta_g \, d\theta_g \, d\phi \, d\epsilon_1 \, d\epsilon_2 \quad (17)$$

where $\Delta_1 = \Delta_2 = 40°$. The results show that in Cu−MCM-41 the ligands are arranged in the complex as shown for molecule II in Figure 1, whereas a coordination geometry is found in the sample Cu−NaY as illustrated by molecule I. These differences in the coordination geometry of tetrapyridine copper(II) can be explained by the interaction of the complex with the flat inner surface of the mesopores in MCM-41 that have a channel diameter of about 30 Å. A relatively strong interaction of the complex with the pore walls is indicated by the results of the room-temperature ESR measurements, which show that the complex is rigid within the time scale of the ESR experiment and presumably attached to the pore walls. If the complex interacts again via the electron system of the pyridine ligands with the flat inner surface of the molecular sieve a coordination

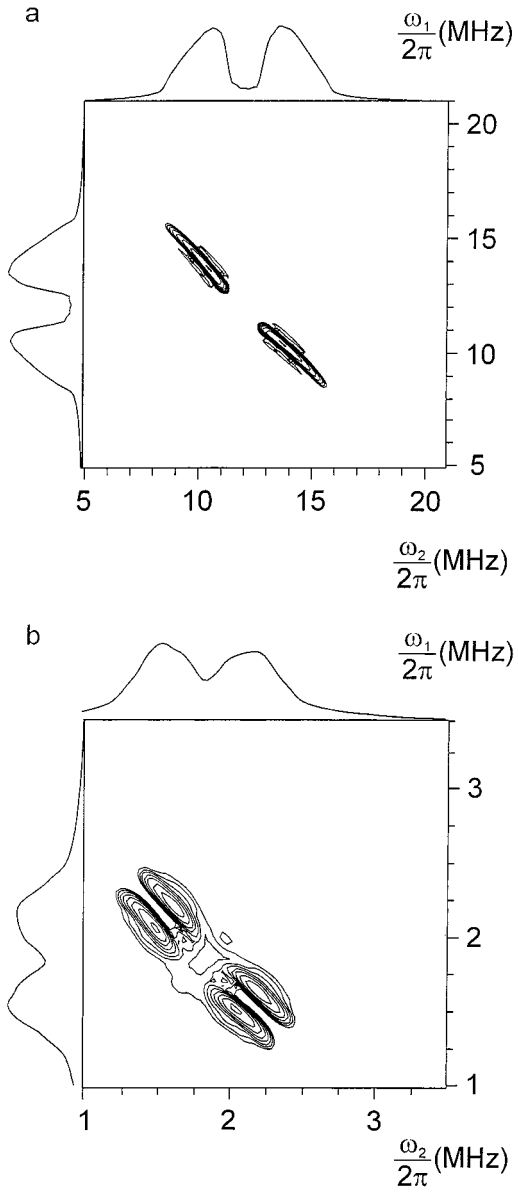

Figure 11. Simulated proton (a) and deuterium (b) HYSCORE spectra of pyridine ligand molecule I with $\epsilon_1 = \epsilon_2 = 0$, $\Delta\epsilon_1 = \Delta\epsilon_2 = 42°$ for an axially symmetric **g** tensor and microwave irradiation at the $g_{||}$ ($\theta_g = 0$) spectral position.

geometry according to molecule II ($\epsilon_1 = \epsilon_2 = 0$) should be preferred. In this case the tetrapyridine copper (II) complex is presumably coordinated with its complex plane parallel to the walls of the mesopores. The distortion of the complex symmetry in the Cu−MCM-41 material as indicated by the strong variance in the angles ϵ_1 and ϵ_2 are more severe than in the Cu−NaY zeolite. It is noteworthy that the large line widths observed in the ESR spectrum of the $[Cu(NC_5H_5)_4]^{2+}$ complex in the sample Cu−MCM-41 indicate likewise substantial distortions of the complex symmetry. It is obvious from sterical arguments that all pyridine ligands cannot be coplanar with the $Cu-N_4$ complex plane.[25] However, this would only account for a variance of approximately 15° in the angles ϵ_1 or ϵ_2. The remaining distortion of the complex symmetry seems to be a direct consequence of the amorphous structure of the walls of the mesopores in the MCM-41 molecular sieves. X-ray studies[33] on siliceous MCM-41 revealed that the inner surface of the MCM-41 walls is highly distorted. The walls are believed to be composed of various more or less dense packed SiO_2 structures. The material density decreases near the surface of the walls, which gives rise to a poor defined border between wall and channel. The substantial disorder in the ligand arrangement suggests likewise heavy distortions of the claimed flat inner surface of the MCM-41 material on a length scale, which is comparable to the maximum dimensions of the tetrapyridine copper (II) complex (12 Å).

The estimated isotropic hf parameter $A_{iso} = 4.1$ MHz of the pyridine protons H2/H6 in Cu−MCM-41 is comparable to those found for tetrapyridine copper(II) complexes in frozen solution[25] and is considerably smaller than that in Cu−NaY. This seems not to be surprising as the influence of electrostatic forces on the electron system of the $[Cu(NC_5H_5)_4]^{2+}$ complex is expected to be comparably small in a frozen pyridine solution and in pure siliceous MCM-41 material with its electrostatic neutral framework. Otherwise, the results obtained for NaY zeolites show that negatively charged frameworks and the associated cations may considerably influence electron distribution within the whole complex.

Conclusions

The 2D ESEEM experiments reveal that different arrangements of the pyridine ligand molecules of the encapsulated tetrapyridine copper(II) complex occur in the two host materials Cu−NaY and Cu−MCM-41. In Cu−NaY zeolites the ligands are predominately arranged with their molecular plane perpendicular to the complex plane. Otherwise, the ligands have a mean orientation of their molecular plane parallel to the complex plane in Cu−MCM-41 materials with severe distortions of the overall complex geometry. The distinct differences in the coordination geometry of the metal complex are a result of the high structural flexibility of the $[Cu(NC_5H_5)_4]^{2+}$ complex and the specific properties of the host materials such as channel dimension and curvature of the inner surface. The bonding system of the pyridine molecule seems to play a key role in the interaction between host framework and encapsulated complex, as for both systems the ligands are arranged parallel to the inner surface of the hosts.

In Y zeolites the distortion of the D_{4h} symmetry of the complex is strongly reduced as the cage dimensions approach the maximum complex dimensions and the crystalline zeolite structure provides well-defined sites for the incorporation of metal ion complexes. The results are in accordance with a location of the tetrapyridine copper(II) complex at the center of the 12-membered ring connecting two supercages in the Y zeolite structure, where the pyridine ligands are aligned parallel with their molecular mirror plane to the walls of the two supercages. In mesoporous siliceous MCM-41 molecular sieve material the tetrapyridine copper (II) complex is coordinated with its complex plane parallel to the walls of the mesopores because of the weak curvature of the inner surface of the mesopores. The amorphous structure and low degree of crystalline order of the MCM-41 pore walls manifest themselves in a pronounced structural disorder in the ligand arrangement of the attached tetrapyridine copper(II) complexes.

The framework of the negatively charged Y zeolite has a substantial impact on the electron system of the encapsulated complex as indicated by the displacement of the spin density into the ligand system, which is not observed in the siliceous MCM-41 material. This result indicate a substantial host−guest interaction in Cu−NaY zeolite.

Acknowledgment. This research was supported by the Deutsche Forschungsgemeinschaft within SFB 294. A. P. and

M. H. are thankful to Prof. L. Kevan, University of Houston, for his support and many valuable discussions and to the U.S. National Science Foundation for financial support during their stay at the University of Houston. The authors are grateful to J. Kupferschmidt and A. Rost, Rechenzentrum der Universität Leipzig, for their help in the implementation of the simulation programs on a parallel computing system.

References and Notes

(1) (a) De Vos, D. E.; Knops-Gerrits, P. P.; Parton, R. F.; Weckhuysen, B. M.; Jacobs P. A.; Schoonheydt, R. A. In *Inclusion Chemistry in Zeolites: Nanoscale Materials by Design*; Herron, N, Corbin, D. R., Eds.; Kluwer Academic Publishers: Dordrecht, 1995; pp 185−207. (b) Dutta, P. K. In *Inclusion Chemistry in Zeolites: Nanoscale Materials by Design*; Herron, N, Corbin, D. R., Eds.; Kluwer Academic Publishers: Dordrecht, 1995; pp 215−228.

(2) Mortier, W.; Schoonheydt, R. *Prog. Solid State Chem.* **1985,** *16*, 1.

(3) Sheu, L. L.; Közinger, H.; Sachtler, W. M. H. *J. Am. Chem. Soc.* **1989,** *111*, 8125.

(4) (a) Kresge, C. T.; Leonowicz, M. E.; Roth, W. J.; Vartuli, J. C.; Beck, J. S. *Nature* **1992,** *359*, 710. (b) Beck, J. S.; Vartuli, J. C.; Roth, W. J.; Leonowicz, M. E.; Kresge, C. T.; Schmitt, K. D.; Chu, C. T.-W.; Olson, D. H.; Shepard, E. W.; McCullen, S. B.; Higgins, J. B.; Schlenker, J. L. *J. Am. Chem. Soc.* **1992,** *114*, 10834.

(5) Casci, J. L. In *Advanced Zeolite Science and Application;* Jansen, J. C., Stöcker, M., Karge, H. G., Weitkamp, J., Eds.; Studies in Surface Science and Catalysis 85; Elsevier: Amsterdam, 1994; pp 329−356.

(6) Chen, C.-Y.; Li, H.-X.; Davis, M. E. *Microporous Mater.* **1993,** *2*, 17.

(7) Ukisu, Y.; Kazusaka, A.; Nomura, M. *J. Mol. Catal.* **1991,** *70*, 165.

(8) Senoda, Y.; Ono, Y. *Zeolites* **1986,** *6*, 209.

(9) Anderson, M. W.; Kevan, L. *J. Phys. Chem.* **1987,** *91*, 4174.

(10) (a) Lee, C. W.; Chen, X.; Kevan, L. *J. Phys. Chem.* **1991,** *95*, 8626. (b) Zamadics, M.; Kevan, L. *J. Phys. Chem.* **1993,** *97*, 10102.

(11) Comets, J.-M.; Kevan, L. *J. Phys. Chem.* **1993,** *97*, 446.

(12) Leith, J. R.; Leach, H. F. *Proc. R. Soc. London, Ser. A* **1972,** *330*, 247.

(13) Vedrine, J. C.; Derouane, E. G.; Ben Taarit, Y. *J. Phys. Chem.* **1974,** *78*, 531.

(14) Dai, P.; Lunsford, J. *J. Inorg. Chem.* **1980,** *19*, 262.

(15) Hartmann, M.; Kevan, L. *J. Chem. Soc., Faraday Trans.* **1996,** *92*, 3661.

(16) Pöppl, A.; Kevan, L. *Langmuir* **1995,** *11*, 4486.

(17) Schweiger, A. In *Structure and Bonding 51*; Springer: Berlin, 1982.

(18) Mims, W. B. In *Electron Paramagnetic Resonance*; Geschwind, S., Ed.; Plenum Press: New York, 1972; pp 263−352.

(19) Kevan, L. *Acc. Chem. Res.* **1987,** *20*, 1.

(20) Kevan, L. In *Time Domain Electron Spin Resonance*; Kevan, L., Schwartz, R. N., Eds.; Wiley: New York, 1979; Chapter 8.

(21) Narayana, M.; Kevan, L. *J. Chem. Soc., Faraday Trans. 1* **1986,** *82*, 213.

(22) Höfer, P.; Grupp, A.; Nebenführ, H., Mehring, M. *Chem. Phys. Lett.* **1986,** *132*, 279.

(23) Höfer, P. *J. Magn. Reson., Ser. A* **1994,** *111*, 77.

(24) Pöppl, A.; Kevan, L. *J. Phys. Chem.* **1996**, *100*, 3387.

(25) Pöppl, A.; Hartmann, M.; Böhlmann, W.; Böttcher, R. *J. Phys. Chem. A* **1998**, *102*, 3599.

(26) Anderson, M. W.; Kevan, L. *J. Phys. Chem.* **1986,** *90*, 6542.

(27) Gemperle, C.; Aebli, G.; Schweiger, A.; Ernst, R. R. *J. Magn. Reson.* **1990,** *88*, 241.

(28) Pöppl, A.; Böttcher, R. *Chem. Phys.* **1997,** *221*, 53.

(29) Harris, R. K.; Mann, B. E. *NMR on the periodic table*; Academic Press: London, 1978.

(30) (a) Hoffman, B. M.; Martinsen, J.; Venters, A. R. *J. Magn. Reson.* **1984,** *59*, 110. (b) Hurst, G. C.; Henderson, T. A.; Kreilick, R. W *J. Am. Chem. Soc.* **1985,** *107*, 7294. (c) Greiner, S. P.; Kreilick, R. W.; Kraft, K. A. *J. Am. Chem. Soc.* **1992,** *114*, 391.

(31) Rist, G. H.; Hyde, J. S. *J. Chem. Phys.* **1969,** *50*, 4532.

(32) Heidler, R.; Janssens, G. O. A.; Mortier, W. J.; Schoonheydt, R. A. *J. Phys, Chem.* **1996,** *100*, 19728.

(33) Elder, K. J.; Reynolds, P. A.; White, J. W.; Cookson, D. *J. Chem. Soc., Faraday Trans.* **1997,** *93*, 199.